Vuorte, Maisa; Vierros, Sampsa; Kuitunen, Susanna; Sammalkorpi, Maria

Adsorption of impurities in vegetable oil: A molecular modelling study

Published in:
Journal of Colloid and Interface Science

DOI:
10.1016/j.jcis.2020.03.012

Published: 01/07/2020

Document Version
Peer-reviewed accepted author manuscript, also known as Final accepted manuscript or Post-print

Please cite the original version:
Vuorte, M., Vierros, S., Kuitunen, S., & Sammalkorpi, M. (2020). Adsorption of impurities in vegetable oil: A molecular modelling study. *Journal of Colloid and Interface Science*, *571*, 55-65.
https://doi.org/10.1016/j.jcis.2020.03.012

Aggregation and adsorption of impurities in triolein on silica substrates: a molecular modelling study

Maisa Vuorte[a], Sampsa Vierros[a,b], Susanna Kuitunen[b], Maria Sammalkorpi[a,c,*]

[a]*Department of Chemistry and Materials Science, School of Chemical Engineering, Aalto University, P.O. Box 16100, FI-00076 Aalto, Finland*
[b]*Neste Engineering Solutions Oy, P.O. Box 310, FI-06101 Porvoo, Finland*
[c]*Department of Bioproducts and Biomaterials, School of Chemical Engineering, Aalto University, P.O. Box 16100, FI-00076 Aalto, Finland*

Abstract

Here, the adsorption of impurity species from triglyceride solvent representing a model vegetable oil is studied using atomistic molecular dynamics simulations. We compare the adsorption of water, glycerol, oleic acid, monoolein, and two types of phospholipids on model silica adsorbents differing in their OH-group density, i.e. hydrogen bonding ability, quartz and cristobalite. We find that the species containing charged groups, phospholipids DOPC and DOPE, adsorb significantly stronger than the nonionic impurities. Secondary contribution to adsorption arises from hydrogen bonding capability of the impurity species, the silica surface, and also the triglyceride solvent: in general, more hydrogen bonding sites in impurity species leads to enhanced adsorption but hydrogen bonding with solvent competes for the available sites. Interestingly, adsorption is weaker on cristobalite even though it has a higher hydrogen bonding site density than quartz. This is because the hydrogen

---

[*] Corresponding author
Email address: `maria.sammalkorpi@aalto.fi` (Maria Sammalkorpi)

bonds can saturate each other on the adsorbent. The finding demonstrates that optimal adsorption response is obtained with intermediate adsorbent hydrogen bonding site densities. Additionally, we find that monoolein and oleic acid show a concentration driven adsorption response and reverse micelle like aggregate formation in bulk triglyceride solvent even in the absence of water. The findings offer insight into adsorption phenomena at inorganic adsorbent - apolar solvent interfaces and provide guidelines for enhanced design of adsorbent materials for example for vegetable oil purification.

Keywords: Molecular dynamics, Adsorption, Aggregation, Vegetable oil, Colloids in oil, CHARMM

1. Introduction

Bio-based oils are an important food staple but also a renewable, environmentally more sustainable replacement to conventional fossil-based crude oils [1–5]. Additionally, they offer a reliable, low toxic, low cost starting material for products of variable structure and functionality, for example paints, coatings, adhesives, synthetic polymers, biomedical glues, drug carriers, and tissue scaffolds [5–8]. In general, bio-based oils are considered a renewable and green option, although their usage in chemical technology remains limited by downstream processing costs [9]. Consequently, the current biggest technical market for vegetable oils comprises of products that are easily attainable from plant-oils, such as detergents and slipping agents [10]; this clearly calls for improvements in the efficiency and control for vegetable oil processing. Here, we focus on an important step in oil purification but also in bio product extraction from plant oils, adsorption of plant oil components to adsorbent.

Although crude vegetable oils consist mainly of triglycerides, they also contain a wide variety of minor components, such as mono- and diglycerides, phospholipids, free fatty acids, fatty acid soaps, colouring pigments, proteins, sterols, free glycerol, and water [11, 12]. These impurities may adversely affect both the manufacturing process and the quantity and quality of plant oil based products, for example by introducing unwanted colour or flavour or shortening the shelf-life of the oil. To reach desirable oil quality for both legislative and industry standards, commonly multi-stage purification processes are employed. These involve steps, such as, washing the oil with water or acid, gravity separation, membrane-based separation, and the use of adsorbents, such as, bleaching earths to dry-wash the oil [1, 3, 13–16]. However, complex multi-step purification processes come with a high energy cost and produce both solid waste and polluted effluents. Additionally, valuable by-products are lost due to destructive treatment of the oil with alkaline reagents.

A very interesting, less destructive alternative for impurity removal from vegetable oils is dry-washing the oil using solid adsorbents. In this approach, the undesired components of the oil adsorb to the adsorbent, and can be removed with it. The approach was originally used to remove chlorophyll and pigments, but it can be used also for selective adsorption of hydrophilic impurity species, such as, glycerol [14], mono- and diglycerides [14], fatty acids [17–19], soaps [19], or phospholipids [20, 21] from the oil. Common adsorbents for the process include, e.g., silicates, silica-based adsorbents, and organo-clays, ion exchange resins, and activated carbon [14, 17, 18, 20, 22, 23].

Although adsorption-based purification of vegetable oils is widely used at industrial scale, molecular level studies of the adsorption phenomena are severely lacking; little is known about the thermodynamics and kinetics underlying the multicomponent adsorption. This is mainly due to challenges of model systems in describing accurately the vegetable oil environment. In particular, the influence of naturally occurring moisture and bulk aggregation of minor chemical species make predicting and interpreting the response challenging [21]. Some molecular level adsorption studies involving vegetable oils do, however, exist. For example, the kinetics and energetics of adsorption processes in vegetable oils on a variety of organo-clay, activated carbon, and mineral surfaces have been described using adsorption isotherms derived based on quartz crystal micro balance (QCM) [24], interferometric surface force apparatus (SFA) [25, 26], rheometry [27], colorimetry [28–31], and Fourier transform infrared spectrosopy (FT-IR) [32]. Furthermore, the formed structures at the oil – solid interface have been characterized using sum frequency spectroscopy (SFS) [33] and x-ray and neutron reflectometry [34–36]. Also computational approaches to the adsorption of surfactants and other organic compounds at the apolar oil – solid interface exist, see e.g. Refs. 37–44. However, adsorption at the water – solid interface, see e.g. Refs. 45–57 has received more attention. Notably the existing computational works reveal that adsorption at the oil – solid interface is affected by a complex interplay of factors, such as, surface chemistry and surface morphology, oil composition, the presence of polar additives, adsorbate saturation, pressure and possible shear forces [37–40].

An important factor influencing both the vegetable oil characteristics and adsorption from the oil is the self-assembly of minority components. The self-assembly of vegetable oil constituents, such as phospholipids, monoglycerides, and to a lesser extent fatty acids and diglycerides, in nonpolar solvents has been studied both experimentally using calorimetry [58, 59], dye solubilization [60], light scattering [61, 62], and small angle X-ray scattering techniques [62–67] but also via computational means [60, 68–73]. The studies reveal that the structure and stability of any aggregates formed in the apolar solvents are highly sensitive to temperature [60, 64, 66], solvent [61, 65, 70], additive concentration [60, 66, 67, 70], as well as, the presence of polar impurities, such as water [60, 67, 69, 72].

Molecular modelling methods provide detailed insight into the entire adsorption process, that is, description of adsorbates diffusion at the surface [74, 75], solvent and adsorbate structure and possible phase transitions at the surface [49, 74–78], as well as, insight into the adsorption and desorption kinetics [74, 79]. Despite the high practical importance of vegetable oils and the well-established oil chemistry and composition dependency of both adsorption and self-assembly in oils, we are not aware of existing molecular modelling works addressing adsorption from vegetable oils. Here, we use molecular modelling methodology to examine systematically adsorption onto two distinct crystalline hydrophilic silica surfaces in model vegetable oil. We compare the adsorption responses of different oil minority components to extract general guidelines for the adsorption in terms of surface activity and adsorbate chemistry. The findings enable drawing conclusions of the adsorption preferences of a variety of components examined, namely water, glycerol, oleic acid, monoolein, and two types of phospholipids. Additionally, we map the effect of surfactant concentration on the aggregation and adsorption preference via comparing monoolein and oleic acid solutions. The results presented in this work offer insight into the molecular interaction mechanisms underlying practical adsorption phenomena in apolar environments and serve as basic guidelines in the development of optimal adsorbent surfaces.

2. Computational methods

The adsorption of water, glycerol, oleic acid, monoolein, dioleoylphosphatidylcholine (DOPC), and dioleoylphosphatidylethanolamine (DOPE) from triolein as model vegetable oil on either α-quartz or α-cristobalite model silica substrates was examined. Adsorption was characterized by determining the potential of mean force (PMF) corresponding to adsorption for single adsorbate molecules. For monoolein and oleic acid, also 5 – 25 wt-% bulk concentrations were examined to resolve the distribution of the surfactants to bulk solution aggregates and adsorbed ones, as well as, characterization of the formed structures. A summary of the structures of the adsorbate species, the solvent triolein, and sample simulation systems are presented in Figure 1. The molecular structures of the two silica adsorbents are presented in Figure 2.

The choice of triolein as a model vegetable oil solvent follows both earlier experimental [80–82] and computational studies [60, 70, 71]. The model adsorbents α-quartz and α-cristobalite were chosen to probe the dependence of vegetable oil additive adsorption on the silica surface silanol (OH-) group density, which can vary between 0.0 OH/nm^2 and 9.4 OH/nm^2. α-quartz corresponds to the maximum possible silanol group density 9.4 OH/nm^2, while on α-cristobalite the silanol group densty is 4.7 OH/nm^2. The selected surface models correspond to silica surfaces present at pH 2–4, where no ionization of the silanol Si–OH groups into siloxide Si–O$^-$ groups takes place [83]. Outside pH range extrema, the degree of ionization of silanol groups on silica can range from 0.0 to 0.2 ionized groups per nm^2, depending on pH, ionic strength of the solution, and surface type [84–87]. The examined adsorbate species comprise a variety of naturally present minority components in plant oils and are selected to provide a broad view on the adsorption response from plant oils.

Gromacs 5.1.5 simulation package [88] was used for the molecular dynamics (MD) simulations. The analysis was done using Gromacs 2016.5. For the biomolecular species, the standard CHARMM C27 force field [89–92] coupled with a united atom solvent representation [93] was used: the triolein alkyl tails were described with the united-atom description, while all-atom description was retained for the headgroups. This enables accurate probing of, e.g., hydrogen bonding which is important for adsorption. The α-quartz and α-cristobalite surfaces were described using the CHARMM C27 compatible silica parametrization by Emami *et al.* [83]. Here, silanol groups, as well as all other surface atoms are mobile, leading to a dynamic hydrogen bonding pattern on of the surface silanol groups. Water was described with the explicit tip3p [94] water model implemented in the CHARMM C27 force field.

In all MD simulations, the Lennard-Jones interactions were truncated at 1.2 nm with a shift to zero between 1.0 and 1.2 nm. The long-range electrostatics employ the PME algorithm with 1.2 nm cut-off, a grid spacing of 0.12 nm, and 4th order splines. All C–H bonds were constrained using the LINCS algorithm. A time step of 2 fs was used. The temperature was controlled using the velocity rescale thermostat by Bussi *et al.* [95] with a coupling constant of $\tau_T = 0.5$ ps and a system reference temperature of 343.15 K. Here, the higher temperature leads to enhanced molecular level dynamics. Particularly, the solvent triolein is relatively viscous and equilibrates slow in comparison to molecular simulations time scale at room temperature. Initial pressure equilibration was done with an isotropic Berendsen barostat [96] ($\tau_p = 1.0$ ps) after which an isotropic Parinnello-Rahman barostat [97, 98] ($\tau_p = 2.0$ ps) was used. For both barostat algorithms, reference pressure of 1 bar and compressibility of 4.5×10^{-5} bar^{-1} were used. For the production MD run, a semi-isotropic version of the Parinnello-Rahman barostat was used, with $\tau_p = 2.0$ ps, a reference pressure of 1.0 bar and compressibility of 4.5×10^{-5} bar^{-1} in both x, y- and z- directions.

The construction of the simulation boxes is detailed in the Supporting information. In brief, first an ideal silica slab 1.7 nm (α-quartz) or 2.5 nm (α-cristobalite) thick were constructed to span the simulation box in the xy-plane. The silica slab also defined the xy-cross section of the simulation box. The examined silica slabs sizes were 3.5 nm × 3.5 nm (3.4 nm × 3.5 nm), 5.0 nm × 5.2 nm (5.1 nm × 5.0 nm), and 7.0 nm × 6.9 nm (6.8 nm × 7.0 nm), where the first number set refers to α-quartz and the set in parenthesis corresponds to α-cristobalite. After this, solvent (single adsorbate simulations) or the bulk concentration adsorbates and the solvent were added, followed by scaling of the simulation box in the z-direction and NPT-equilibration, such that a random mixture with density matching closely with density calculated

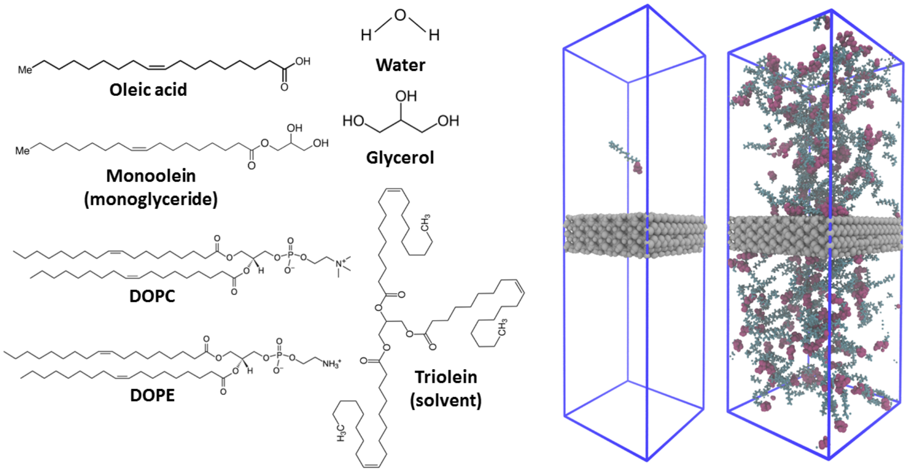

Figure 1: Left: molecular structures of the surfactant and solvent compounds used in this work. Right: Sample initial configurations corresponding to the single molecule and bulk adsorption simulation set-ups used in this work. The snapshots correspond to a single monoolein and 15 wt-% monoolein in triolein with a quartz surface in simulation boxes of size $5.0 \times 5.2 \times 18.5$ nm^3 and $7.0 \times 6.9 \times 19.6$ nm^3. For clarity, the triolein solvent has been omitted form the visualizations.

based on densities of pure components from literature [99, 100] was obtained. In the single adsorbate simulations, the adsorbate is originally 6 nm above the silica substrate. The details of the protocols are provided in Supporting information. A summary of the system sizes and compositions is available as Table S1 of Supporting information.

For single adsorbate systems, the umbrella sampling starting configurations were generated by pulling the adsorbate from bulk solution towards the silica surface center of mass. A pull rate of 1 nm/ns with harmonic constraint $k = 40000$ kJ mol^{-1} nm^{-2} was used. The pull group consisted of the hydrophilic headgroup of the adsorbate or the entire molecule for water

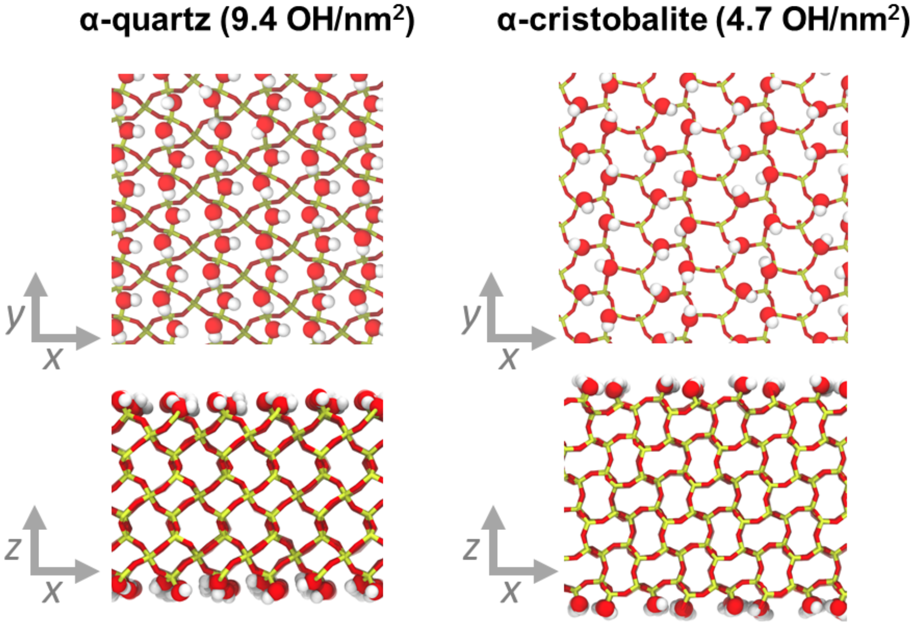

Figure 2: Visualisations of the x, y- and x, z-profiles of the α-quartz and α-cristobalite silica adsorbents used in this work. The atom types are differentiated by colour so that oxygen is red, silicon yellow, and hydrogen white.

and glycerol. Umbrella sampling starting configurations were extracted from the pull trajectory based on the distance of the adsorbate from the silica surface at 0.2 nm intervals. A 500 – 3500 kJ mol^{-1} nm^{-2} harmonic constraint was enforced on the adsorbate and each window was simulated for 100 – 300 ns following the NPT setup described previously. The potential of mean force (PMF) profiles correspond to the average of 300 bootstrapped profiles and the WHAM analysis developed by Kumar et al. [101] was used in extracting the PMF. Error estimate is based on standard deviation of the 300 bootstrapped PMF profiles.

For simulations of 5–25 wt-% monoolein or oleic acid, the production simulation was an NPT molecular dynamics simulation 500 ns in duration. Analysis was performed on the last 200 ns as the mean structural quantities have reached a stable state for that time period.

For analysis, the existence of a hydrogen bond was determined based on a cut-off distance of 0.35 nm between the acceptor and the donor atoms. A cut-off angle of 30^o was used. The lifetime τ_b of the hydrogen bonds was estimated as the correlation time, that is, the integral of the hydrogen bond autocorrelation function $C(\tau)$ [102]:

$$\tau_b = \int_0^\infty C(\tau) d\tau \tag{1}$$

The surfactant aggregate size and adsorption classification was carried out based on distance-based cut-offs, following Ref. 70. A summary of the classification is that if any atoms of the polar headgroups of two surfactants were within R_{cut} of one another, the surfactants were considered to be part of the same aggregate. Similarly, any atom of the polar headgroups residing within R_{cut} of the silanol groups of the silica surface indicated adsorption. A cut-off distance of $R_{cut} = 3.2$ Å was used in the classification. The aggregate size distribution and adsorbed fraction was calculated in 20 ns sequential windows over the analyzed 200 ns simulation time period. The reported final aggregate size distribution and amount of adsorbed surfactants represents an average over all the windows. Error of the distributions was estimated based on the standard deviation of the 20 ns distributions. Molar concentrations of aggregates were calculated based on the oil (triolein solvent and surfactant mixture) volume. The oil volume was determined by subtracting the volume of the silica slab, approximated based on the van der Waals radii [103] of the surface atoms, from the total volume of the simulation box.

3. Results and discussion

First, the adsorption of single surfactants onto two different crystalline silica surfaces, α-quartz and α-cristobalite, was examined using steered MD-simulations and umbrella sampling to resolve estimates of the free energy profile corresponding to adsorption of water, glycerol, monoolein, oleic acid, triolein, and the two phospholipid species (DOPE and DOPC). From it, the free energy of adsorption ΔE_{ads} was determined. A summary of the obtained adsorption energy values for the different adsorbate species and surfaces is available as Figure 3. Figure 3 also presents a sample free energy profile, i.e. potential of mean force (PMF) curve, determined for water on quartz and cristobalite with the adsorption energy ΔE_{ads} marked. The other corresponding potential of mean force curves are presented in the Supporting information.

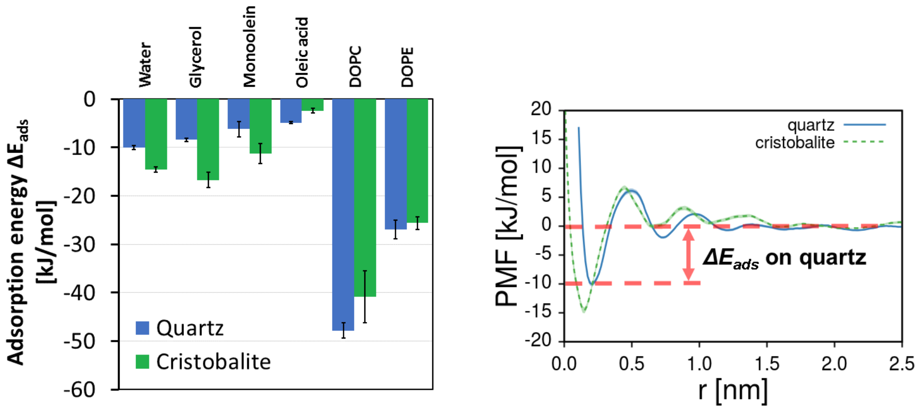

Figure 3: Free energies of adsorption ΔE_{ads} for water, glycerol, monoolein, oleic acid, DOPC, and DOPE on quartz and cristobalite surfaces (left). The error estimates correspond to ± standard deviation. Example PMF curve (water on quartz and cristobalite) with the reported adsorption energy ΔE_{ads} marked (right).

The data in Figure 3 shows that both surfactant and surface type have a strong effect on adsorption strength. Generally, the adsorption of the two species with charged groups, i.e. the phospholipids DOPC and DOPE, is much stronger than the adsorption of the nonionic species. For the examined nonionic species (water, glycerol, monoolein, oleic acid), with the exception of oleic acid, higher adsorption energies are observed for adsorption on cristobalite than on quartz. For oleic acid on cristobalite, the adsorption energy appears very small. Superficially, this observed general preference of adsorption on cristobalite over quartz appears counter-intuitive as quartz has a significantly higher density of silanol (hydroxy) groups (9.4 OH/nm^2) than cristobalite (4.7 OH/nm^2). However, in addition to hydrogen bonding with the adsorbate, the surface silanol OH-groups can form hydrogen bonds also at the surface. This requires a small enough, optimally $2.5 - 2.8$ Å, separation distance between the silanol groups [104, 105]. At distances greater than 3.1 Å , the silanol groups are considered incapable of hydrogen bonding with one another [104]. Notably, as the free, not already hydrogen bonded, silanol groups function as main adsorption sites on the silica surface, adsorption is not governed by the concentration of silanol groups but actually the concentration of free silanol groups [104]. Furthemore, on most silica adsorbents, the silanol group concentration is far from uniform. While strong hydrogen bonding between surface silanol groups is expected on quartz, on cristobalite the lower OH-group density prevents the formation of hydrogen bonding between the surface silanol groups. This leaves the sites free for contributing to adsorption which shows in the data of Figure 3. Altogether, this means that besides charge, adsorption strength is sensitive also to the silanol group density of the surface, as well as, to the ability of the surfactant to form hydrogen bonds with the triolein solvent.

Oleic acid adsorption response differs from these general charge and hydrogen bonding ability based observations. The weak adsorption of oleic acid on cristobalite is likely explained by two contributing factors, i.e. molecular flexibility of oleic acid and the hydrogen bonding patterns facilitated by the lower OH-group density on cristobalite. Oleic acid is a large, highly flexible molecule and carboxylic acid headgroup adopts easily a multitude of configurations. Coupled with the flexible geometry of the surface silanol groups, the flexibility of oleic acid results in a high number of possible adsorption geometries on both quartz and cristobalite. Extrapolating based on the modes of adsorption of smaller carboxylic acids onto silica from both gas phase and aqueous solution, oleic acid can be expected to form either one or two hydrogen bonds between its carboxylic acid group and the surface silanol groups [18, 106, 107]. The formation of either one or two hydrogen bonds at the surface is predominantly dictated by the OH-group density of the surface; the sparser OH-group density of cristobalite does not facilitate adsorption of oleic acid via two simultaneous hydrogen bonds.

The adsorption energies of the two charged phospholipids, DOPC and DOPE, are significantly higher when compared to nonionic adsorbates. The structures of the DOPC and DOPE include identical fatty acid tails and a negatively charged phosphate group, whereas the structure of the positively charged headgroup moiety differs slightly between a choline group (DOPC) and a ethanolamine group (DOPE). As a result of this structural difference, similar PC and PE phospholipids differ greatly in their phase transition and aggregation properties [108–110]. In comparison to the choline head group, the ethanolamine headgroup can also function as a hydrogen bond donor. This enables DOPE to form hydrogen bonds also with the surrounding triolein solvent, which most likely contributes to its lower adsorption energy when compared to DOPC. Interestingly, both DOPC and DOPE show a minimal preference for adsorption onto quartz over cristobalite.

Notably, the CHARMM C27 force field overestimates the partial charges of phospholipid headgroups [111, 112]. As a result of this, the adsorption energies of DOPC and DOPE reported here are overestimated in comparison to the uncharged species.

To examine the effect of aggregation and interactions between the adsorbing surfactants, bulk adsorption and aggregation of two model surfactants differing in their hydrogen bonding capability, monoolein and oleic acid, was examined over a bulk concentration range. Figure 4 presents the average number of the surfactant molecules adsorbed at the silica–triolein interface as a function of surfactant concentration. Surfactant adsorption increases nearly linearly with increased surfactant concentration within the examined concentration range in these systems. This indicates saturation coverage is not reached within the examined concentrations. Only with monoolein adsorption on quartz the adsorption deviates from linear concentration dependency indicating the presence of already adsorbed species start to have a nonlinear influence. For all systems, the data shows the adsorbed coverages remain below saturation coverages. Additionally, as will be further discussed, aggregation of monolein and oleic acid occurs at least partly as aggregates. The above makes estimation of the saturation coverage for either of the examined surfactants based purely on hydrophilic headgroup size or fitting of a Langmuir isotherm model to the data based on the calculated energies of adsorption (see Figure 3) impractical. Both surfactants adsorb more on cristobalite than quartz and monoolein adsortion exceeds oleic acid on both examined adsorbents. For monoolein, the response is consistent with the adsorption energies of individual surfactants, see Figure 3. However, for oleic acid the bulk adsorption response exceeds significantly what would be expected based on the individual surfactant adsorption energies. Furthemore, oleic acid adsorbs more on cristobalite than on quartz in these bulk systems, opposed to the individual surfactant adsorption energy values. The reason for these is that the single surfactant adsorption energies do not take into account cooperative effects driving oleic acid adsorption. As the analysis below reveals, oleic acid forms dimers in the bulk triolein solvent and adsorption as dimers is preferential.

To enable further analysis of the adsorption response, Figure 5 shows the average number of hydrogen bonds per surfactant molecule as the function of surfactant concentration. The data shows that monoolein molecules have an average of approximately 0.2 intramolecular H-bonds per molecule independent of concentration (oleic acid does not form intramolecular hydrogen bonds). However, the degree of intermolecular hydrogen bonding for both surfactants steadily increases with concentration while surfactant – triolein hydrogen bonding decreases. This means that intermolecular surfactant – surfactant hydrogen bonds gradually replace surfactant – triolein hydrogen bonds with increasing surfactant concentration. It also means that both monoolein and oleic acid prefer aggregation over solvation by triolein. Our

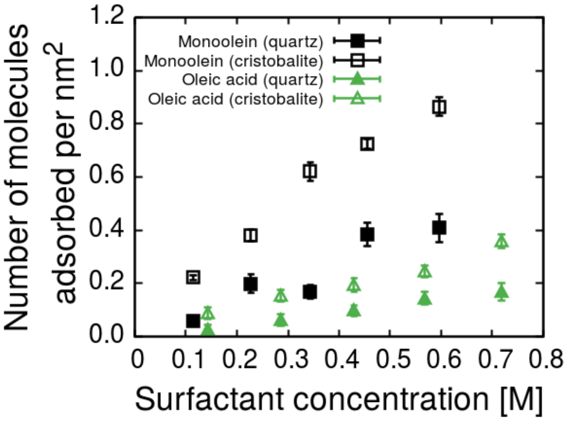

Figure 4: Number of molecules of oleic acid and monoolein adsorbed at the silica–triolein interface (quartz or cristobalite) per surface area of adsorbent as a function of surfactant concentration. Error bars correspond to ± standard deviation.

earlier work [70] addresses this bulk aggregation response more in detail.

The corresponding hydrogen bond life-times τ_b have been presented in Table 1. Table 1 shows that the lifetime of the monoolein – monoolein hydrogen bonds increases with monoolein concentration. This results from stabilization of the bonds by the structure of larger monoolein aggregates. Conversely, the lifetime of oleic acid – oleic acid intermolecular hydrogen bonds, while notably longer lasting, decreases with oleic acid concentration. This is mostly explained by carboxylic acid tendency to dimerize in apolar solutions via cooperatively stabilized hydrogen bonds [113–117], while larger aggregates remain unfavourable [70].

The longer lifetimes and greater number of surfactant – surface hydrogen bonds on cristobalite compared to quartz reflect the adsorption preference on cristobalite. Despite increased adsorption of monoolein at higher surfactant concentrations, see Figure 4, the average number of monoolein – surface hydrogen bonds decreases as a function of monoolein concentration. This may indicate adsorption of monoolein aggregates on the surface, as has been previously computationally observed by Bradley-Shawn *et al.* in mica nanopores [39, 40]. Conversely, hydrogen bonding of oleic acid with the adsorbent remains at a constant level throughout the examined concentration range.

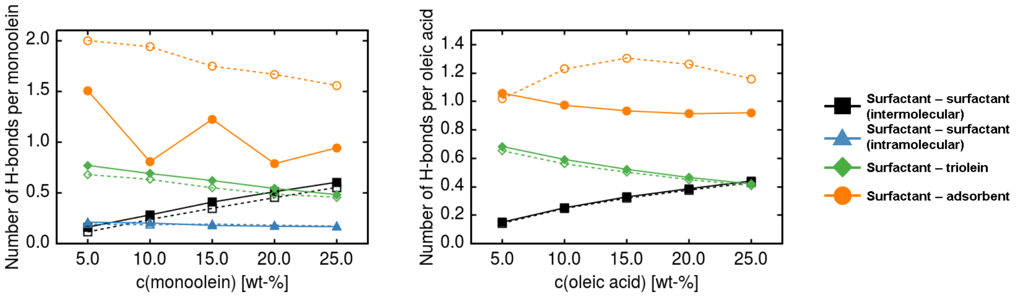

Figure 5: Average number of hydrogen bonds formed per monoolein (left) and oleic acid (right) molecules. Data normalization is by the number of surfactants (intermolecular and intramolecular bonds) or by the number of adsorbed surfactants (bonds with adsorbent). The filled symbols and solid lines correspond to simulations on quartz ans the open symbols and dashed lines to simulations on cristobalite.

Figure 6 presents the aggregate size distributions of monoolein and oleic acid for systems containing the quartz and cristobalite surfaces. On the employed logarithmic scale, the distributions corresponding to both surfactants are quite linear, i.e. correspond to exponential size distribution, at small aggregate sizes and low concentrations. However, the monoolein distribution becomes skewed towards larger aggregates at surfactant concentrations above

Table 1: Hydrogen bond average lifetimes τ_b for monoolein–triolein and oleic acid-triolein systems at varying surfactant bulk wt-% concentration c on silica.

		τ_b [ps]		
c(monoolein) [wt-%]	adsorbent	monoolein–monoolein	monoolein–triolein	monoolein–surface
5	quartz	432	459	532
10	quartz	460	414	573
15	quartz	423	426	660
20	quartz	520	443	612
25	quartz	527	422	647
5	cristobalite	683	706	3624
10	cristobalite	756	678	3475
15	cristobalite	757	626	3915
20	cristobalite	759	538	3635
25	cristobalite	678	516	3647
c(oleic acid) [wt-%]	adsorbent	oleic acid–oleic acid	oleic acid–triolein	oleic acid–surface
5	quartz	1671	713	396
10	quartz	1644	686	449
15	quartz	1586	685	454
20	quartz	1478	673	409
25	quartz	1311	639	453
5	cristobalite	1875	719	1498
10	cristobalite	1636	705	1422
15	cristobalite	1513	695	1292
20	cristobalite	1402	686	1285
25	cristobalite	1342	649	1417

10-wt-%. The systematically slightly smaller aggregates in the cristobalite containing systems are explained by the smaller effective bulk concentration of the surfactant due to stronger adsorption at the surface.

Furthermore, Figure 7 presents the average aggregation numbers and the concentration of unimers of monoolein and oleic acid at different bulk surfactant concentrations. The aggregate and unimer data corresponds to the

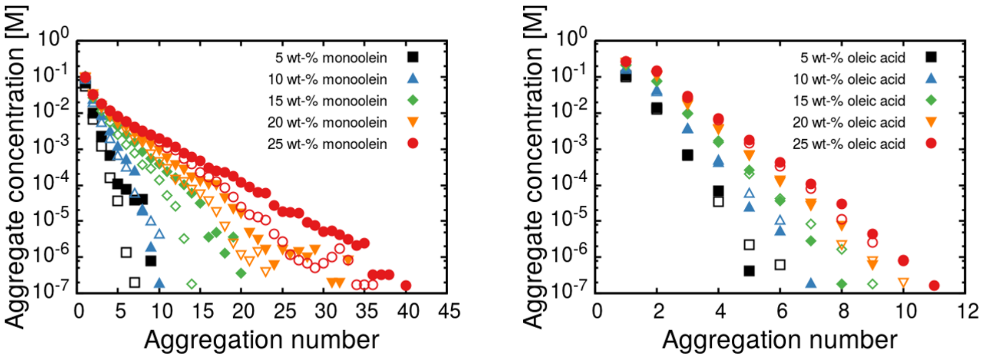

Figure 6: Aggregate size distributions in the bulk triolein solvent for monoolein (left) and oleic acid (right). The y-axis concentration is the molar concentration of aggregate size n in solution. Filled symbols correspond to simulation systems containing a quartz surface and open symbols to systems with cristobalite surface.

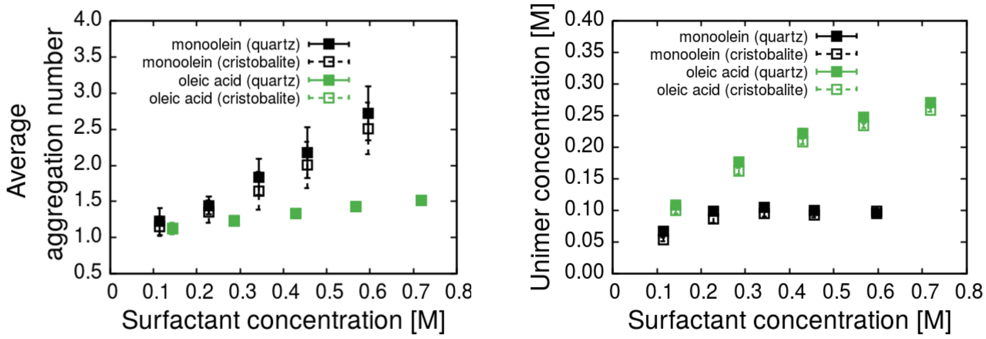

Figure 7: Average aggregation number (left) and surfactant unimer (unaggregated surfactant) concentrations (right) as a function of surfactant concentration for monoolein and oleic acid in triolein. The data presents the aggregates in bulk solution, i.e. the adsorbed surfactants are not included. Filled symbols correspond to quartz and open symbols to cristobalite systems. Errorbars correspond to ± standard deviation.

surfactants remaining in bulk triolein solution, i.e. the adsorbed surfactants are omitted. The surfactant concentration is the total surfactant concentration. The data shows that for both systems, the average aggregation number

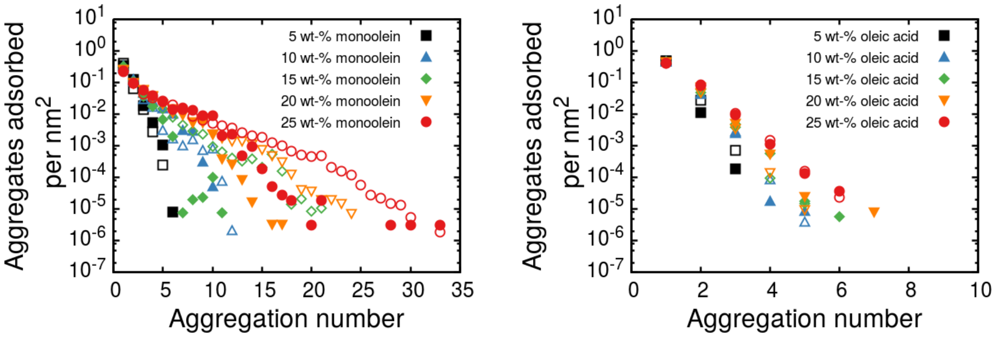

Figure 8: Aggregate size distributions (number of aggregates of given size adsorbed on adsorbent surface per nm^2) for monoolein (left) and oleic acid (right) adsorbed at the silica surface. Filled symbols correspond to quartz and open symbols to cristobalite systems.

increases steadily with total surfactant concentration. For monoolein, the aggregate size is more sensitive to the concentration while oleic acid aggregates increase in size only modestly. Notably, a majority of the surfactants remain as unimers and the aggregates remain very small which is consistent with prior reports of aggregation response of related biospecies, see e.g. Refs. 70. Examination of the free unimer concentration reveals that for both surfactants, the unimer concentration first steadily increases with concentration. However for oleic acid, the unimer concentration keeps increasing steadily, while for monoolein a plateau in the unimer concentration is reached already at $\sim$ 0.2 M surfactant total concentration. Such response is characteristic with the onset of micellization in systems exhibiting a CMC, and is consistent with the data in Figure 6.

In general, an exponential aggregate size distribution is characteristic of surfactant systems following a classical open association model in which the aggregates grow step-wise and the aggregation steps have equal association energy involved [118, 119]. Notably, such aggregation response indicates the system does not have a clear critical micellization concentration (CMC) even though aggregates form. See Ref. 70 for a detailed discussion of aggregation models in related apolar solvent - surfactant systems. Conversely, if the system shows a preferred micelle size, i.e. aggregates of some specific size being favored energetically, the aggregation response corresponds to closed association type aggregation models. Closed association aggregation models describe the classical aqueous surfactant system micellization response where a peaked micelle size distribution at concentrations above a CMC is present.

The data of Figure 6 supported by Figure 7 leads to the conclusion that oleic acid aggregation follows within this examined concentration range very closely open association, and no CMC like response can be expected. Oleic acid aggregation following an open-association model is further supported by the gradual growth in aggregate size with increased surfactant concentration. This can be seen both from the shift in the aggregate size distribution in Figure 6 and also from the increase in average aggregation number in Figure 7. Additionally, the aggregation of oleic acid in triolein is limited to the formation of small oligomers.

Also for monoolein, the aggregation response is dominantly open association but at elevated concentrations the monoolein systems start showing preference for formation of larger aggregates. Additionally, the aggregates formed by monoolein are larger than those formed by the oleic acid due to the greater hydrogen bonding capability of the monoolein headgroup compared to oleic acid. The here observed monoolein aggregate growth with concentration is in agreement with experimental characterization of diglycerol monolaurate and monomyristate reverse micelles in olive oil by Shrestha *et al.* [66]. Likewise, the deviation from purely exponential growth toward larger aggregate sizes follows the findings for monopalmitin by Vierros *et al.* [70].

Figure 8 presents the size distribution of monoolein and oleic acid aggregates that have been adsorbed at the quartz or cristobalite surface. Compared to the bulk solution aggregate distributions presented in Figure 6, the aggregates at the silica surface are smaller. However, this is very likely explained by the slower diffusion of larger aggregates to the surface and the limited simulation time. However, the monoolein aggregates on the cristobalite surface are systematically larger than those on quartz. Oleic acid aggregate adsorption does not show such differences between cristobalite and quartz. The enhanced adsorption of larger aggregates on cristobalite explains largely the difference in monoolein adsorption between cristobalite and quartz in Figure 4. Notably, the enhanced monoolein aggregate adsorption has an onset concentration at 10 wt-% which corresponds to monoolein aggregates with aggregation number exceeding ten becoming prevalent.

4. Conclusions

Here, the surface adsorption and bulk aggregation behaviour of a series of model vegetable oil components was examined through molecular modelling with the aim of extracting systematic molecular level information of features influencing e.g. selective extraction of the components via adsorbates, harvesting biospecies or dry-washing the oil. We conclude that the largest contribution to adsorption preference of individual surfactants comes from whether the surfactant contains charged groups, i.e. the two examined phospholipid species adsorb very strongly in comparison to the other examined polar or polar group containing species. Besides surfactant charge, adsorption from the model plant oil is strongly influenced by the ability of the adsorbing species to form hydrogen bonds either with the adsorbent (promotes adsorption) or with the triglyceride solvent (competes with adsorption). Additionally, via comparing two model adsorbents differing in their hydrogen bonding density, we were able to conclude that simple chemical treatments, for example introducing OH-groups or analogous hydrothermal or acid treatments of the adsorbent can be used to effectively tune the adsorption efficiency.

However, interestingly, an increased amount of binding sites on the adsorbent does not necessarily lead to increased adsorption as the binding sites may interact with each other: for example, the results here show that binding energy associated with the charged or polar species adsorption on cristobalite (silanol group density of 4.7 $\mathrm{OH/nm^2}$) exceeds that of quartz (silanol group density of 9.4 $\mathrm{OH/nm^2}$) because on the quartz surface, the silanol groups are so densely that they saturate themselves. This leads to an effectively lower free OH group density than on cristobalite. At a practical level, this means that there exists an optimal surface density of adsorbate binding sites for maximizing adsorption efficiency. Finally, a comparison of individual surfactant and bulk solution adsorption response shows how collective behavior can promote adsorption. Namely, comparison of monoolein and oleic acid aggregation and adsorption responses show that competition between the surfactant-surfactant aggregation in the solvent vs adsorption as single surfactants or aggregates is the key in governing adsorption: while individual oleic acid molecules remain well solvated in the triglyceride solvent, in bulk solution they form also oligomers and these oligomers prefer adsorption to remaining solvated.

At a more detailed level, the two examined charged phospholipids adsorbed very strongly on both quartz and cristobalite, with the adsorption driven by the charged groups of the surfactants. However, the non-ionic species preferred adsorption on cristobalite over quartz. For the non-ionic species, adsorption strength shows sensitivity to surface OH-group density. On the examined quartz surface that has a high OH-group density, the surface OH-groups are able to hydrogen bond with one another, thus decreasing the density of free OH groups on the surface in comparison to cristobalite where hydrogen bonding between the OH-groups at the surface does not occur. This leads to adsorption on cristobalite, that has the intermediate binding site density, being favourable to adsorption over quartz that has a higher adsorption site density. Finally, additive adsorption at the silica surface is affected by the ability of the adsorbate to hydrogen bond with the surrounding triolein solvent.

The effect of surfactant concentration on both adsorption and aggregation phenomena was examined on 5 – 25 wt-% monoolein or oleic acid in triolein solutions with either quartz or cristobalite surface. Both surfactants exhibited increased adsorption on cristobalite over quartz, despite contradictory small energies of adsorption for oleic acid, with evidence of aggregate adsorption at the surface. Additionally, we discovered a significant, surfactant concentration dependent bias towards larger monoolein aggregates adsorbing on cristobalite compared to quartz. A majority of the surfactant molecules form aggregates in the bulk solvent. The formed aggregates, especially in the case of monoolein, were filament like, and highly dynamic with no clearly shielded core, differing greatly from the expected structure of reverse micelles. The aggregation of oleic acid was mostly limited to formation of small oligomers. For both oleic acid and monoolein, average aggregation number increased with surfactant concentrations, with the formation of larger aggregates being more energetically favoured at high monoolein concentrations.

Overall this work provides useful, bottom up insight to aggregation and adsorption characteristics and behaviour of both fundamentally and technologically very important, renewable biobased oil systems. To our knowledge, these results are the first microscopic level detailed characterization of the adsorption and aggregation of either uncharged or charged surfactant species on inorganic surfaces in non-polar solvent environments. Additionally, the study was performed on a technologically highly relevant solvent, a model vegetable oil. Based on the results, we are able to draw general guidelines with potential practical significance, e.g. connecting the presence of an optimal, intermediate density adsorption site density to strongest adsorption. Altogether, the work provides insight into understanding of the interactions of vegetable oils and their components at liquid – solid interface, as well as, guidelines for the design of efficient adsorbent materials for use in biospecies harvesting or vegetable oil purification processes. Additionally, the highly specific tunability of monoglyceride and fatty acid aggregate size and shape through variation of factors such as surfactant and water concentration, temperature, and surfactant structure, underlines the potential of these systems in a wide variety of applications, including use as microreactors and in drug delivery systems [64–66, 70].

5. Acknowledgements

This work was partly financed by the Fortum Foundation projects 201800097 and 20190199. The authors acknowledge the financial support of the Academy of Finland Grant No. 309324 (M.S.). We are grateful for the support by the FinnCERES Materials Bioeconomy Ecosystem. Computational resources by CSC IT Centre for Science, Finland, and RAMI – RawMatTERS Finland Infrastructure are also gratefully acknowledged.

References

[1] Z. J. Predojevic, The production of biodiesel from waste frying oils: A comparison of different purification steps, Fuel 87 (2008) 3522 – 3528.

[2] J. McNeill, Y. Kakuda, B. Kamel, Improving the quality of used frying oils by treatment with activated carbon and silica, J. Am. Oil Chem. Soc. 63 (1986) 1564–1567.

[3] M. Berrios, M. A. Martin, A. F. Chica, A. Martin, Purification of biodiesel from used cooking oils, Appl. Energy 88 (2011) 3625 – 3631.

[4] R. Priambodo, T.-C. Chen, M.-C. Lu, A. Gedanken, J.-D. Liao, Y.-H. Huang, Novel technology for bio-diesel production from cooking and waste cooking oil by microwave irradiation, Energy Procedia 75 (2015) 84–91.

[5] G. Lligadas, J. C. Ronda, M. Galia, V. Cadiz, Renewable polymeric materials from vegetable oils: a perspective, Mater. Today 16 (2013) 337 – 343.

[6] Y. Xia, R. C. Larock, Vegetable oil-based polymeric materials: synthesis, properties, and applications, Green Chem. 12 (2010) 1893–1909.

[7] J. C. Ronda, G. Lligadas, M. Galià, V. Cádiz, Vegetable oils as platform chemicals for polymer synthesis, Eur. J. Lipid Sci. Technol. 113 (2011) 46–58.

[8] L. M. de Espinosa, M. A. Meier, Plant oils: The perfect renewable resource for polymer science?!, Eur. Polym. J. 47 (2011) 837–852.

[9] P. Vennestrøm, C. M. Osmundsen, C. Christensen, E. Taarning, Beyond petrochemicals: the renewable chemicals industry, Angew. Chem. Int. Ed. 50 (2011) 10502–10509.

[10] A. S. Carlsson, J. L. Yilmaz, A. G. Green, S. Stymne, P. Hofvander, Replacing fossil oil with fresh oil - with what and for what?, Eur. J. Lipid Sci. Technol. 113 (2011) 812–831.

[11] J. Orsavova, L. Misurcova, J. V. Ambrozova, R. Vicha, J. Mlcek, Fatty acids composition of vegetable oils and its contribution to dietary energy intake and dependence of cardiovascular mortality on dietary intake of fatty acids, Int. J. Mol. Sci. 16 (2015) 12871–12890.

[12] E. Yara-Varon, Y. Li, M. Balcells, R. Canela-Garayoa, A. S. Fabiano-Tixier, F. Chemat, Vegetable oils as alternative solvents for green oleo-

extraction, purification and formulation of food and natural products, Molecules 22 (2017).

[13] M. Berrios, R. L. Skelton, Comparison of purification methods for biodiesel, Chem. Eng. J. 144 (2008) 459 – 465.

[14] V. A. Mazzieri, C. R. Vera, J. C. Yori, Adsorptive properties of silica gel for biodiesel refining, Energy Fuels 22 (2008) 4281–4284.

[15] M. Rossi, M. Gianazza, C. Alamprese, F. Stanga, The role of bleaching clays and synthetic silica in palm oil physical refining, Food Chem. 82 (2003) 291 – 296.

[16] F. Hussin, M. K. Aroua, M. A. W. Wan Daud, Textural characteristics, surface chemistry and activation of bleaching earth: A review, Chem. Eng. J. 170 (2011) 90 – 106.

[17] D. R. Taylor, C. B. Ungermann, Z. Demidowicz, The adsorption of fatty acids from vegetable oils with zeolites and bleaching clay/zeolite blends, J. Am. Oil Chem. Soc. 61 (1984) 1372–1379.

[18] U. Kalapathy, A. Proctor, A new method for free fatty acid reduction in frying oil using silicate films produced from rice hull ash, J. Am. Oil Chem. Soc. 77 (2000) 593–598.

[19] P. Assawasaengrat, P. Jintanavasan, P. Kitchaiya, Adsorption of ffa, soap and glycerine in biodiesel using magnesium silicate, Chem. Eng. Trans. 43 (2015) 1135–1140.

[20] M. Laatikainen, W. Srithammavut, B. Toukoniitty, I. Turunen, T. Sainio, Phospholipid adsorption from vegetable oils on acid-activated sepiolite, Adsorption 21 (2015) 409–417.

[21] S. M. Silva, K. A. Sampaio, R. Ceriani, R. Verhe, C. Stevens, W. De Greyt, A. J. A. Meirelles, Adsorption of carotenes and phosphorus from palm oil onto acid activated bleaching earth: equilibrium, kinetics and thermodynamics, J. Food Eng. 118 (2013) 341 – 349.

[22] A. B. Fadhil, M. M. Dheyab, A. Y. Abdul-Qader, Purification of biodiesel using activated carbons produced from spent tea waste, J. Assoc. Arab Univ. Basic Appl. Sci. 11 (2012) 45 – 49.

[23] D. F. Stout, L. E.and Chamberlain, J. M. McKelvey, Factors influencing vegetable oil bleaching by adsorption, J. Am. Oil Chem. Soc. 26 (1949) 120–126.

[24] K. O. Evans, G. Biresaw, Quartz crystal microbalance investigation of the structure of adsorbed soybean oil and methyl oleate onto steel surface, Thin Solid Films 519 (2010) 900–905.

[25] A. Proctor, C. Adhikari, G. D. Blyholder, Lipid adsorption on commercial silica hydrogels from hexane and changes in triglyceride complexes with time, J. Am. Oil Chem. Soc. 73 (1996) 693–698.

[26] S. M. Lundgren, M. Ruths, K. Danerlöv, K. Persson, Effects of unsaturation on film structure and friction of fatty acids in a model base oil, J. Colloid Interface Sci. 326 (2008) 530–536.

[27] G. Biresaw, A. Adhvaryu, S. Erhan, C. Carriere, Friction and adsorption properties of normal and high-oleic soybean oils, J. Am. Oil Chem. Soc. 79 (2002) 53.

[28] J. Mingyu, A. Proctor, The effect of added solvents on soy oil lutein adsorption by silicic acid, J. Am. Oil Chem. Soc. 70 (1993) 575–578.

[29] H. G. Brown, H. E. Snyder, Adsorption of soy oil phospholipids on silica, J. Am. Oil Chem. Soc. 62 (1985) 753–756.

[30] M. Ribeiro, P. Lourenço, J. Monteiro, S. Ferreira-Dias, Kinetics of selective adsorption of impurities from a crude vegetable oil in hexane to activated earths and carbons, Eur. Food Res. Technol. 213 (2001) 132–138.

[31] K. Boki, M. Kubo, N. Kawasaki, H. Mori, Adsorption isotherms of pigments from alkali-refined vegetable oils with clay minerals, J. Am. Oil Chem. Soc. 69 (1992) 372–378.

[32] C. Adhikari, A. Proctor, G. Blyholder, Diffuse-reflectance fourier-transform infrared spectroscopy of vegetable oil triglyceride adsorption on silicic acid, J. Am. Oil Chem. Soc. 71 (1994) 589–594.

[33] M. T. Casford, P. B. Davies, The structure of oleamide films at the aluminum/oil interface and aluminum/air interface studied by Sum Frequency Generation (SFG) vibrational spectroscopy and Reflection Absorption Infrared Spectroscopy (RAIRS), ACS Appl. Mater. Interfaces 1 (2009) 1672–1681.

[34] B. Luokkala, S. Garoff, R. Suter, Using x-ray reflectivity to determine the structure of surfactant monolayers, Phys. Rev. E 62 (2000) 2405.

[35] M. Campana, A. Teichert, S. Clarke, R. Steitz, J. R. Webster, A. Zarbakhsh, Surfactant adsorption at the metal–oil interface, Langmuir 27 (2011) 6085–6090.

[36] M. H. Wood, R. J. Welbourn, T. Charlton, A. Zarbakhsh, M. Casford, S. M. Clarke, Hexadecylamine adsorption at the iron oxide–oil interface, Langmuir 29 (2013) 13735–13742.

[37] M. Doig, P. J. Camp, The structures of hexadecylamine films adsorbed on iron-oxide surfaces in dodecane and hexadecane, Phys. Chem. Chem. Phys. 17 (2015) 5248–5255.

[38] M. Doig, C. P. Warrens, P. J. Camp, Structure and friction of stearic acid and oleic acid films adsorbed on iron oxide surfaces in squalane, Langmuir 30 (2013) 186–195.

[39] J. L. Bradley-Shaw, P. J. Camp, P. J. Dowding, K. Lewtas, Molecular Dynamics Simulations of Glycerol Monooleate Confined between Mica Surfaces, Langmuir 32 (2016) 7707–7718.

[40] J. L. Bradley-Shaw, P. J. Camp, P. J. Dowding, K. Lewtas, Self-assembly and friction of glycerol monooleate and its hydrolysis products in bulk and confined non-aqueous solvsent, Phys. Chem. Chem. Phys. 20 (2018) 17648–17657.

[41] S. J. Eder, A. Vernes, G. Betz, On the derjaguin offset in boundary-lubricated nanotribological systems, Langmuir 29 (2013) 13760–13772.

[42] Y. Xiong, T. Cao, Q. Chen, Z. Li, Y. Yang, S. Xu, S. Yuan, J. Sjöblom, Z. Xu, Adsorption of a polyaromatic compound on silica surfaces from organic solvents studied by molecular dynamics simulation and afm imaging, J. Phys. Chem. C 121 (2017) 5020–5028.

[43] J. Zhong, P. Wang, Y. Zhang, Y. Yan, S. Hu, J. Zhang, Adsorption mechanism of oil components on water-wet mineral surface: A molecular dynamics simulation study, Energy 59 (2013) 295 – 300.

[44] Q. Liu, S. Yuan, H. Yan, X. Zhao, Mechanism of oil detachment from a silica surface in aqueous surfactant solutions: molecular dynamics simulations, J. Phys. Chem. B 116 (2012) 2867–2875.

[45] R. Tosaka, H. Yamamoto, I. Ohdomari, T. Watanabe, Adsorption mechanism of ribosomal protein L2 onto a silica surface: a molecular dynamics simulation study, Langmuir 26 (2010) 9950–9955.

[46] N. R. Tummala, L. Shi, A. Striolo, Molecular dynamics simulations of surfactants at the silica–water interface: Anionic vs nonionic headgroups, J. Colloid Interface Sci. 362 (2011) 135 – 143.

[47] K. Shah, P. Chiu, M. Jain, J. Fortes, B. Moudgil, S. Sinnott, Morphology and mechanical properties of surfactant aggregates at water–silica interfaces: molecular dynamics simulations, Langmuir 21 (2005) 5337–5342.

[48] K. Shah, P. Chiu, S. B. Sinnott, Comparison of morphology and mechanical properties of surfactant aggregates at water–silica and water–

graphite interfaces from molecular dynamics simulations, J. Colloid Interface Sci. 296 (2006) 342 – 349.

[49] G. Srinivas, S. O. Nielsen, P. B. Moore, M. L. Klein, Molecular dynamics simulations of surfactant self-organization at a solid-liquid interface, J. Am. Chem. Soc. 128 (2006) 848–853.

[50] A. Rimola, D. Costa, M. Sodupe, J. F. Lambert, P. Ugliengo, Silica surface features and their role in the adsorption of biomolecules: computational modeling and experiments, Chem. Rev. 113 (2013) 4216–4313.

[51] S. Aslan, J. Määttä, B. Z. Haznedaroglu, J. P. M. Goodman, L. D. Pfefferle, M. Elimelech, E. Pauthe, M. Sammalkorpi, P. R. Van Tassel, Carbon nanotube bundling: influence on layer-by-layer assembly and antimicrobial activity, Soft Matter 9 (2013) 2136–2144.

[52] J. Määttä, S. Vierros, P. R. Van Tassel, M. Sammalkorpi, Size-selective, noncovalent dispersion of carbon nanotubes by pegylated lipids: A coarse-grained molecular dynamics study, J. Chem. Eng. Data 59 (2014) 3080–3089.

[53] J. Määttä, S. Vierros, M. Sammalkorpi, Controlling carbon-nanotube-phospholipid solubility by curvature dependent self-assembly, J. Phys. Chem. B 119 (2015) 4020–4032.

[54] M. Sammalkorpi, A. Z. Panagiotopoulos, M. Haataja, Surfactant and hydrocarbon aggregates on defective graphite surface: Structure and dynamics, J. Phys. Chem. B 112 (2008) 12954–12961.

[55] M. Sammalkorpi, A. Z. Panagiotopoulos, M. Haataja, Structure and dynamics of surfactant and hydrocarbon aggregates on graphite: A molecular dynamics simulation study, J. Phys. Chem. B 112 (2008) 2915–2921.

[56] N. R. Tummala, A. Striolo, Sds surfactants on carbon nanotubes: Aggregate morphology, ACS Nano 3 (2009) 595–602.

[57] N. R. Tummala, A. Striolo, Role of counterion condensation in the self-assembly of sds surfactants at the water–graphite interface, J. Phys. Chem. B 112 (2008) 1987–2000.

[58] K. Kon-No, T. Jin-No, A. Kitahara, Solubility, critical aggregating or micellar concentration, and aggregate formation of nonionic surfactants in nonaqueous solutions, J. Colloid Interface Sci. 49 (1974) 383–389.

[59] J. Jagur-Grodzinski, R. Frame, R. M. Izatt, Inverted micelles of monoolein in decalin: calorimetric determination of equilibriuim constants and degrees of association, J. Colloid Interface Sci. 105 (1985) 73–79.

[60] O. P. Lehtinen, R. W. N. Nugroho, T. Lehtimaa, S. Vierros, P. Hiekkataipale, J. Ruokolainen, M. Sammalkorpi, M. Österberg, Effect of temperature, water content and free fatty acid on reverse micelle formation of phospholipids in vegetable oil, Colloids Surf. B Biointerfaces 160 (2017) 355–363.

[61] P. Debye, W. Prins, Micellar dispersion of α-monoglycerides in benzene and chlorobenzene, J. Colloid Sci. 13 (1958) 86–98.

[62] L. K. Shrestha, M. Dulle, O. Glatter, K. Aramaki, Structure of polyglycerol oleic acid ester nonionic surfactant reverse micelles in decane: growth control by headgroup size, Langmuir 26 (2010) 7015–7024.

[63] P. A. Penttilä, S. Vierros, K. Utriainen, N. Carl, L. Rautkari, M. Sammalkorpi, M. Österberg, Phospholipid-Based Reverse Micelle Structures in Vegetable Oil Modified by Water Content, Free Fatty Acid, and Temperature, Langmuir 35 (2019) 8373–8382.

[64] L. K. Shrestha, T. Sato, D. P. Acharya, T. Iwanaga, K. Aramaki, H. Kunieda, Phase behavior of monoglycerol fatty acid esters in nonpolar oils: reverse rodlike micelles at elevated temperatures, J. Phys. Chem. B 110 (2006) 12266–12273.

[65] L. K. Shrestha, O. Glatter, K. Aramaki, Structure of nonionic surfactant (glycerol alpha-monomyristate) micelles in organic solvents: a SAXS study, J. Phys. Chem. B 113 (2009) 6290–6298.

[66] L. K. Shrestha, G. R. Shrestha, K. Aramaki, Self-assembled structures of diglycerol monolaurate- and monomyristate in olive oil, J. Dispersion Sci. Technol. 30 (2009) 1525–1532.

[67] L. K. Shrestha, M. Kaneko, T. Sato, D. P. Acharya, T. Iwanaga, H. Kunieda, Phase behavior of diglycerol fatty acid esters-nonpolar oil systems, Langmuir 22 (2006) 1449–1454.

[68] S. Vierros, M. Sammalkorpi, Phosphatidylcholine reverse micelles on the wrong track in molecular dynamics simulations of phospholipids in an organic solvent, J. Chem. Phys. 142 (2015) 094902.

[69] S. Vierros, M. Sammalkorpi, Role of hydration in phosphatidylcholine reverse micelle structure and gelation in cyclohexane: a molecular dynamics study, Phys. Chem. Chem. Phys. 17 (2015) 14951–14960.

[70] S. Vierros, M. Österberg, M. Sammalkorpi, Aggregation response of triglyceride hydrolysis products in cyclohexane and triolein, Phys. Chem. Chem. Phys. 20 (2018) 27192–27204.

[71] S. Vierros, M. Sammalkorpi, Hybrid atomistic and coarse-grained model for surfactants in apolar solvents, ACS Omega 4 (2019) 15581–15592.

[72] S. Abel, N. Galamba, E. Karakas, M. Marchi, W. H. Thompson, D. Laage, On the Structural and Dynamical Properties of DOPC Reverse Micelles, Langmuir 32 (2016) 10610–10620.

[73] G. Folpini, T. Siebert, M. Woerner, S. Abel, D. Laage, T. Elsaesser, Water Librations in the Hydration Shell of Phospholipids, J. Phys. Chem. Lett. 8 (2017) 4492–4497.

[74] R. Hentschke, R. G. Winkler, Molecular dynamics simulation study of the adsorption of chain alkanes from solution onto graphite, J. Chem. Phys. 99 (1993) 5528–5534.

[75] A. Jabbarzadeh, J. D. Atkinson, R. I. Tanner, Wall slip in the molecular dynamics simulation of thin films of hexadecane, J. Chem. Phys. 110 (1999) 2612–2620.

[76] H. Dominguez, Self-aggregation of the SDS surfactant at a solid-liquid interface, J. Phys. Chem. B 111 (2007) 4054–4059.

[77] T. K. Xia, U. Landman, Molecular dynamics of adsorption and segregation from an alkane mixture, Science 261 (1993) 1310–1312.

[78] T. Desai, P. Keblinski, S. K. Kumar, Computer simulations of the conformations of strongly adsorbed chains at the solid–liquid interface, Polymer 47 (2006) 722 – 727.

[79] V. Zhdanov, B. Kasemo, Monte carlo simulation of the kinetics of protein adsorption, Proteins 30 (1998) 177–182.

[80] F. Mori, J. C. Lim, O. G. Raney, C. M. Elsik, C. A. Miller, Phase behavior, dynamic contacting and detergency in systems containing triolein and nonionic surfactants, Colloids Surf. 40 (1989) 323 – 345.

[81] K. Maeda, H. Kuramochi, T. Fujimoto, Y. Asakuma, K. Fukui, M. Osako, K. Nakamura, S.-i. Sakai, Phase equilibrium of biodiesel compounds for the triolein + palmitic acid + methanol system with dimethyl ether as cosolvent, J. Chem. Eng. Data 53 (2008) 973–977.

[82] F. Peyronel, J. Ilavsky, G. Mazzanti, A. G. Marangoni, D. A. Pink, Edible oil structures at low and intermediate concentrations. ii. ultra-small angle x-ray scattering of in situ tristearin solids in triolein, J. Appl. Phys. 114 (2013) 234902.

[83] F. S. Emami, V. Puddu, R. J. Berry, V. Varshney, S. V. Patwardhan, C. C. Perry, H. Heinz, Force field and a surface model database for silica to simulate interfacial properties in atomic resolution, Chem. Mater. 26 (2014) 2647–2658.

[84] S. V. Patwardhan, F. S. Emami, R. J. Berry, S. E. Jones, R. R. Naik, O. Deschaume, H. Heinz, C. C. Perry, Chemistry of aqueous silica nanoparticle surfaces and the mechanism of selective peptide adsorption, J. Am. Chem. Soc. 134 (2012) 6244–6256.

[85] W. A. House, D. R. Orr, Investigation of the ph dependence of the kinetics of quartz dissolution at 25 c, J. Chem. Soc. Faraday Trans. 88 (1992) 233–241.

[86] D. E. Yates, T. W. Healy, The structure of the silica/electrolyte interface, J. Colloid Interface Sci. 55 (1976) 9–19.

[87] S. K. Milonjić, Determination of surface ionization and complexation constants at colloidal silica/electrolyte interface, Colloids Surf. 23 (1987) 301–312.

[88] M. J. Abraham, T. Murtola, R. Schulz, S. Pall, J. C. Smith, B. Hess, E. Lindahl, Gromacs: High performance molecular simulations through multi-level parallelism from laptops to supercomputers, SoftwareX 1-2 (2015) 19 – 25.

[89] S. E. Feller, D. Yin, R. W. Pastor, A. D. MacKerell, Molecular dynamics simulation of unsaturated lipid bilayers at low hydration: parameterization and comparison with diffraction studies, Biophys. J. 73 (1997) 2269–2279.

[90] P. Bjelkmar, P. Larsson, M. A. Cuendet, B. Hess, E. Lindahl, Implementation of the CHARMM force field in GROMACS: analysis of

protein stability effects from correction maps, virtual interaction sites, and water models, J. Chem. Theory Comput. 6 (2010) 459–466.

[91] N. Foloppe, A. D. MacKerell, All-atom empirical force field for nucleic acids: I. parameter optimization based on small molecule and condensed phase macromolecular target data, J. Comput. Chem. 21 (2000) 86–104.

[92] A. D. MacKerell, N. K. Banavali, All-atom empirical force field for nucleic acids: Ii. application to molecular dynamics simulations of DNA and RNA in solution, J. Comput. Chem. 21 (2000) 105–120.

[93] J. Henin, W. Shinoda, M. L. Klein, United-atom acyl chains for CHARMM phospholipids, J. Phys. Chem. B 112 (2008) 7008–7015.

[94] H. J. C. Berendsen, J. R. Grigera, T. P. Straatsma, The missing terms in effective pair potentials, J. Phys. Chem. 91 (1987) 6269–6271.

[95] G. Bussi, D. Donadio, M. Parrinello, Canonical sampling through velocity rescaling, J. Chem. Phys. 126 (2007) 014101.

[96] H. J. C. Berendsen, J. P. M. Postma, W. F. Vangunsteren, A. Dinola, J. R. Haak, Molecular-dynamics with coupling to an external bath, J. Chem. Phys. 81 (1984) 3684–3690.

[97] M. Parrinello, A. Rahman, Polymorphic transitions in single-crystals – a new molecular-dynamics method, J. Appl. Phys. 52 (1981) 7182–7190.

[98] M. Parrinello, A. Rahman, P. Vashishta, Structural transitions in superionic conductors, Phys. Rev. Lett. 50 (1983) 1073–1076.

[99] M. J. E. O'Neil, The Merck Index: An Encyclopedia of Chemicals, Drugs, and Biologicals, 14th Revised edition, Elsevier Health Sciences, London, United Kingdom, 2006.

[100] R. E. Weast, Handbook of Chemistry and Physics. 69th ed., CRC Press, Boca Raton, FL, 1988.

[101] S. Kumar, J. M. Rosenberg, D. Bouzida, R. H. Swendsen, P. A. Kollman, The weighted histogram analysis method for free-energy calculations on biomolecules. I. The method, J. Comput. Chem. 13 (1992) 1011–1021.

[102] D. van der Spoel, P. J. van Maaren, P. Larsson, N. Timneanu, Thermodynamics of hydrogen bonding in hydrophilic and hydrophobic media, J. Phys. Chem. B 110 (2006) 4393–4398.

[103] A. Bondi, van der Waals volumes and radii, J. Phys. Chem. 68 (1964) 441–451.

[104] E. Papirer, Adsorption on silica surfaces, Surfactant Science Series, Marcel Dekker, Inc., New York, NY, 2000.

[105] G. Pimentel, A. L. McClellan, The Hydrogen Bond, A Series of chemistry books, W. H. Freeman and Company, New York, NY, 1960.

[106] K. Marshall, C. H. Rochester, Infrared study of the adsorption of

oleic and linolenic acids onto the surface of silica immersed in carbon tetrachloride, J. Chem. Soc., Faraday Trans. 1 71 (1975) 1754–1761.

[107] G. Blyholder, C. Adhikar, A. Proctor, Structure and orientation of oleic acid adsorbed onto silica gel, Colloids Surf. A Physicochem. Eng. Asp. 105 (1995) 151 – 158.

[108] S. Leekumjorn, A. K. Sum, Molecular simulation study of structural and dynamic properties of mixed DPPC/DPPE bilayers, Biophys. J. 90 (2006) 3951–3965.

[109] A. Blume, R. J. Wittebort, S. K. Das Gupta, R. G. Griffin, Phase equilibria, molecular conformation, and dynamics in phosphatidylcholine/phosphatidylethanolamine bilayers, Biochemistry 21 (1982) 6243–6253.

[110] J. M. Boggs, G. Rangaraj, K. M. Koshy, Effect of hydrogen-bonding and non-hydrogen-bonding long chain compounds on the phase transition temperatures of phospholipids, Chem. Phys. Lipids 40 (1986) 23 – 34.

[111] J. B. Klauda, R. M. Venable, J. A. Freites, J. W. O'Connor, D. J. Tobias, C. Mondragon-Ramirez, I. Vorobyov, A. D. MacKerell, R. W. Pastor, Update of the CHARMM all-atom additive force field for lipids: validation on six lipid types, J. Phys. Chem. B 114 (2010) 7830–7843.

[112] C. J. Hogberg, A. M. Nikitin, A. P. Lyubartsev, Modification of the CHARMM force field for DMPC lipid bilayer, J. Comput. Chem. 29 (2008) 2359–2369.

[113] A. Katchalsky, H. Eisenberg, S. Lifson, Hydrogen bonding and ionization of carboxylic acids in aqueous solutions, J. Am. Chem. Soc. 73 (1951) 5889–5890.

[114] E. E. Schrier, M. Pottle, H. A. Scheraga, The influence of hydrogen and hydrophobic bonds on the stability of the carboxylic acid dimers in aqueous solution, J. Am. Chem. Soc. 86 (1964) 3444–3449.

[115] C. Colominas, J. Teixido, J. Cemeli, F. J. Luque, M. Orozco, Dimerization of carboxylic acids: Reliability of theoretical calculations and the effect of solvent, J. Phys. Chem. B 102 (1998) 2269–2276.

[116] A. J. Beveridge, G. C. Heywood, A quantum mechanical study of the active site of aspartic proteinases, Biochemistry 32 (1993) 3325–3333.

[117] G. Pistolis, C. M. Paleos, A. Malliaris, Molecular recognition in organic solvents. the importance of excimer fluorescence spectroscopy, J. Phys. Chem. 99 (1995) 8896–8902.

[118] I. A. Nyrkova, A. N. Semenov, Multimerization: closed or open association scenario?, Eur. Phys. J. E: Soft Matter Biol. Phys 17 (2005) 327–337.

[119] I. A. Nyrkova, A. N. Semenov, On the theory of micellization kinetics, Macromol. Theory Simul. 14 (2005) 569–585.